A NEW COMPUTATIONALLY EFFICIENT STOCHASTIC APPROACH FOR BUILDING RECONSTRUCTION FROM SATELLITE DATA

Florent Lafarge[1,2], Mélanie Durupt[2], Xavier Descombes[1], Josiane Zerubia[1] and Marc Pierrot-Deseilligny[2]

[1] Ariana Research Group, INRIA - 2004, routes des Lucioles, BP93 - 06902 Sophia Antipolis, France - Firstname.Name@inria.fr
[2] French Mapping Agency (IGN) - 2/4 avenue Pasteur - 94165 Saint-Mande, France - Firstname.Name@ign.fr

Commission III, Working Group III/4

KEY WORDS: Reconstruction, Urban, DEM, Satellite, structural approach, MCMC

ABSTRACT:

We present a 3D building reconstruction method from satellite images based on a stochastic approach. It consists in reconstructing buildings by assembling simple urban structures extracted from a library of 3D parametric models, as a LEGO® game. Such a method is particularly well adapted to data of average quality such as high resolution satellite images. The approach is based on a density formulation defined within a Bayesian framework. The configuration which maximizes this density is found using a RJMCMC sampler which is efficient w.r.t. the multiple parametric object recognition problem. Experimental results are shown on complex buildings and dense urban areas using PLEIADES simulations.

1. INTRODUCTION

Three dimensional models of urban areas are very useful for many kinds of applications such as urban planning, radiowave reachability tests for wireless communications or disaster recovery. However the 3D building reconstruction is a difficult problem, mainly due to the complexity of the urban scenes.

Problem statement Many automatic methods have been developed using various kinds of data. Multiple view images are the most common inputs. Such data allow to efficiently extract 3D information in a scene. In (Scholze, Moons, and Van Gool, 2002), 3D-lines are extracted and then grouped into faces which allow to reconstruct buildings through a semantic interpretation. Rooftop hypothesis are generated from 3D-lines and junction information in (Kim and Nevatia, 2004). (Baillard, Schmid, Zisserman, and Fitzgibbon, 1999) presents a method based on planar facet hypothesis which can be generated from a single 3D-line. (Taillandier and Deriche, 2004) combines several kinds of primitives such as 3D-lines, planes and facade hypothesis. These methods provide convincing 3D-models using aerial images. Laser scanning is also very popular since the decrease of the acquisition cost and the accuracy of the measures. Some interesting models have been proposed using laser data such as (Maas and Vosselman, 1999; Haala and Brenner, 1999).
With the recent progress in the spatial domain, this problem can nowadays be tackled by the sub-metric satellite images. Such data are very interesting, especially for the developing countries where the aerial and terrestrial data acquisitions are often difficult and the cadastral maps do not exist. However, such data have "relatively low" resolution and SNR to deal with 3D reconstruction problems. For example, the satellite images used in this paper have 2 pixels per square meter density (i.e. 0.7 meter resolution) contrary to aerial images used in (Baillard, Schmid, Zisserman, and Fitzgibbon, 1999; Scholze, Moons, and Van Gool, 2002) which have about 150 pixels per square meter. Consequently, the satellite context is different and the aerial methods are not especially adapted. For example, the algorithm of (Taillandier and Deriche, 2004) has been tested on such satellite data: a lack of robustness in the primitive extraction does not allow to obtain good results. In this paper, we present a new stochastic method adapted to such satellite data.

Global strategy There are two main families of approaches in 3D building reconstruction. The first one corresponds to generic modelings. These kinds of approaches are theoretically able to reconstruct any shape of building through connected planar facets. However, they demand high resolution data. The second one is the parametric modelings. Although these reconstructions are limited (most of parametric modelings consider a symmetric two-plan roof reconstruction), they are known to be robust with respect to the quality of the data (Weidner and Forstner, 1995).
In this paper, we use an approach which is halfway between generic and parametric modelings : the structural approach. It consists in reconstructing buildings by merging simple urban structures extracted from a library of 3D parametric models, as a LEGO® game (see Fig.1). This approach is particularly interesting since it combines the advantages of both generic and parametric modelings:
1- the robustness of parametric approaches is preserved since the objects of libraries are defined by parameter sets,
2- a library of quality allows to reconstruct a large range of buildings. It is even possible to reconstruct buildings that some generic modelings cannot such as the curved roof structures.

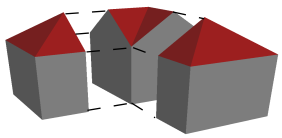

Figure 1. Principle of the structural approach.

However, this approach is based on an important prior knowledge concerning urban structures and their assembling. It is necessary to correctly define these interactions to have a convincing modeling without artefact. A stochastic framework is especially well adapted to introduce such knowledge. (Lafarge, Descombes, Zerubia, and Pierrot-Deseilligny, 2006b) have proposed such a structural approach. This work suffers from several drawbacks: 1-the generation of many artefacts, 2-a lack of 3D-modeling genericity, 3-the tuning of many parameters, and 4-important computing times. In this paper, we propose a new method, based on the same approach but correcting all these drawbacks.
The input of the proposed method is Digital Elevation Models (DEMs) which are well adapted to global geometric descriptions. First, the building footprints are extracted from DEMs using the works of (Ortner, Descombes, and Zerubia, 2007) and (Lafarge, Descombes, Zerubia, and Pierrot-Deseilligny, 2006a). Then, buildings are reconstructed through a density formulation defined in a Bayesian framework. The configuration which maximizes this

density is found using the RJMCMC sampler which is efficient w.r.t. the multiple parametric object recognition problem. Finally, results are shown and evaluated on complex buildings and dense urban areas.

2. BUILDING EXTRACTION

The works of (Ortner, Descombes, and Zerubia, 2007) and (Lafarge, Descombes, Zerubia, and Pierrot-Deseilligny, 2006a) are used to extract the building footprints from DEMs. In (Lafarge, Descombes, Zerubia, and Pierrot-Deseilligny, 2006b), the building footprints were modeled by rectangle layouts (see Fig.2-(c)) estimated by marked point processes (Ortner, Descombes, and Zerubia, 2007). Such footprints generate many artefacts in the 3D reconstruction stage. (Lafarge, Descombes, Zerubia, and Pierrot-Deseilligny, 2006a) proposes to regularize these rectangular footprints by improving the connections between the neighboring rectangles and detecting the facade discontinuities (see Fig.2-(d)). The obtained footprints are configurations of connected quadrilaterals (i.e. quadrilaterals with common edges). Each one is a specific part of a building (a footprint is an unspecified quadrilateral which can even be a triangle). We use these footprints in order to define the 3D-model supports of the structural approach.

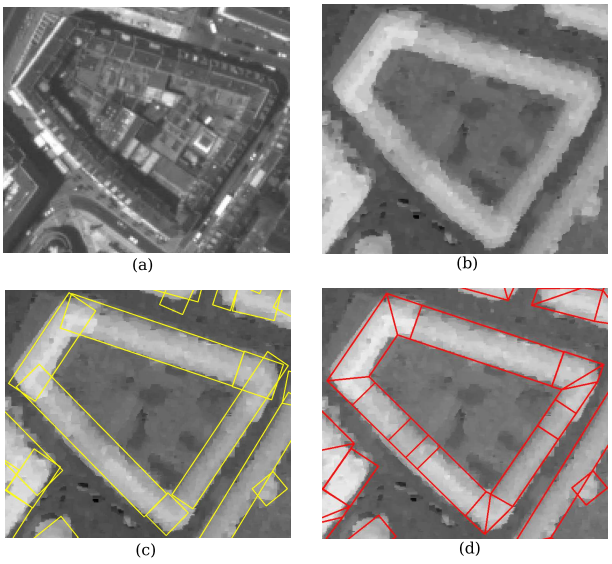

Figure 2. Satellite image of a building **(a)**, associated DEM **(b)**, rectangular footprints **(c)**, and quadrilateral footprints **(d)**.

3. 3D RECONSTRUCTION

3.1 library of 3D-models

The contents of the library is a key point. If the library is too limited (such as in (Lafarge, Descombes, Zerubia, and Pierrot-Deseilligny, 2006b) where only flat and gable roof models are available), the method loses genericity. The proposed library, denoted by $\mathcal{M}$ and presented in Fig.3, allows to reconstruct a large range of buildings through a collection of models. Each model is defined by both a roof form and a variant :

- The proposed roof forms (denoted by $\mathcal{F}$ and illustrated in Figure 3-top) include monoplane roofs ($\mathcal{F}_{1x}$), multi-plane roofs ($\mathcal{F}_{2x}$) and curved roofs ($\mathcal{F}_{3x}$). Each roof form has a specific set of parameters F which the number varies between 1 and 6.
- The variants (denoted by $\mathcal{V}$ and shown in Figure 3-bottom for a gable roof type) are specific to a roof form. They correspond to cases of structure ends (hipped / straight ends) or structure junctions (junctions in "-","L","T" or "+"). The variants allow also to specify the orientation of the roof with respect to the quadrilateral 2D support. The parameter set of the variant, denoted by V, has a dimension varying between 0 and 2.

To sum-up, each model of the library $\mathcal{M}$ is given by a couple $(\mathcal{F}, \mathcal{V})$ and its parameters are given by $\theta = (F, V)$. Details on this library can be found in (Lafarge, 2007). Some models can be degenerated in some situations[1]: these cases are not allowed in the process in practice.

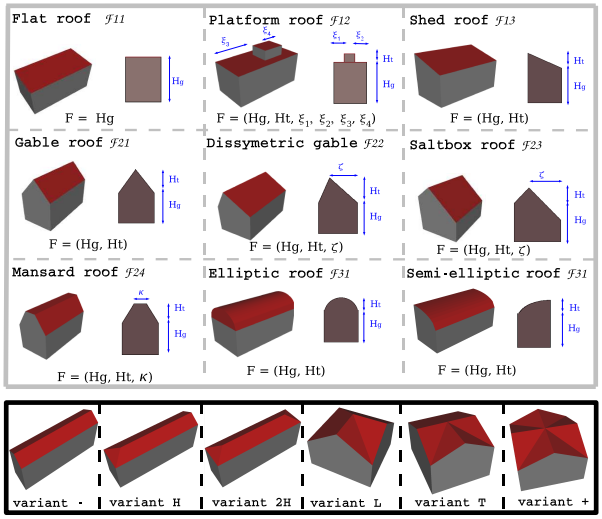

Figure 3. The library of 3D-models - the roof forms (3D and profile views) *(top)*, the variants in the case of a gable roof type *(bottom)*

3.2 Density formulation

The energy formulation requires notations, summarized below:

- S, a set of sites and $\Lambda = \{\Lambda(s)/s \in S\}$, a given DEM where $\Lambda(s)$ represents the intensity of the site s.
- $\mathcal{C}$, the quadrilateral configuration representing the building footprints associated with Λ. N represents the number of quadrilaterals (see Fig. 2-(d)).
- S_i, the subset of S whose sites are inside the quadrilateral $i \in \mathcal{C}$.
- $\mathcal{D} = \{\Lambda(s)/s \in S_i\ , i \in \mathcal{C}\}$, the set of data
- x, an element of the state space $\mathcal{T}$ which corresponds to a configuration of 3D-parametric objects knowing the quadrilateral footprints $\mathcal{C}$. $x = (x_i)_{i\in\mathcal{C}} = (m_i, \theta_i)_{i\in\mathcal{C}}$ where each object x_i is defined by both a model $\mathcal{M}_{m_i}$ of the library $\mathcal{M}$ and a set of parameters θ_i associated with $\mathcal{M}_{m_i}$. In the following, $x_i = (m_i, \theta_i)$ and $\mathcal{M}_{m_i}$ will be respectively called an object and a model.

[1] for example, a semi-elliptic roof on a triangular support

- d_m, the number of parameters of the model $\mathcal{M}_m$.
- $\mathcal{S}_{x_i}$, the function from S_i to $\mathbb{R}$ which associates the roof altitude of the object x_i to each site of S_i.

Let us consider the measurable spaces $(\Omega_n, \mathcal{A}_n, \upsilon_n)$ associated with the Lebesgue measure on $\mathbb{R}^n$ where $n \in \mathbb{N}^\star$. By denoting the characteristic function $\mathbb{1}_{\{.\}}$, the measure associated with the parameters of a model $\mathcal{M}_{m_i} \in \mathcal{M}$ is then given by :

$$\mu_i(x_i) = \sum_{k \in \mathbb{N}^\star} \mathbb{1}_{\{m_i = k\}} \nu_{d_k}(\theta_i) \quad (1)$$

Let us now consider the measurable space $(\mathcal{T}, \mathcal{B}(\mathcal{T}), \mu(.))$ related to the state space $\mathcal{T}$ where $\mu = \mu_1 \times ... \times \mu_N$. We consider the random variable X distributed in $\mathcal{T}$ which follows an unnormalized density $h(.)$ against $\mu(.)$. $h(.)$ is actually the posterior density of a configuration x of objects, given $\mathcal{D}$. In a Bayesian framework, this density can be obtained as follows :

$$h(x) = h(x/\mathcal{D}) \propto h_p(x)\mathcal{L}(\mathcal{D}/x) \quad (2)$$

A requirement is to be able to build both a prior density $h_p(x)$ and a likelihood $\mathcal{L}(\mathcal{D}/x)$. In the following, these two terms are explained.

3.21 Likelihood The likelihood represents the probability of observing the data $\mathcal{D}$ knowing the configuration x. By considering the hypothesis of conditional independence, it can be expressed through the local likelihood of objects $\mathcal{L}(\mathcal{D}_i/x_i)$ as :

$$\mathcal{L}(\mathcal{D}/x) = \prod_{i \in \mathcal{C}} \mathcal{L}(\mathcal{D}_i/x_i) \propto \prod_{i \in \mathcal{C}} \exp -\Gamma^\alpha_{(i)}(\mathcal{S}_{x_i}, \mathcal{D}_i) \quad (3)$$

where $\Gamma^\alpha_{(i)}(.,.)$ is the distance from $\mathbb{R}^{card(S_i)} \times \mathbb{R}^{card(S_i)}$ to $\mathbb{R}$ defined by :

$$\Gamma^\alpha_{(i)}(\mathcal{S}_{x_i}, \mathcal{D}_i) = \left(\sum_{s \in S_i} |\mathcal{S}_{x_i}(s) - \Lambda(s)|^\alpha \right)^{\frac{1}{\alpha}} \quad (4)$$

To resume, the likelihood corresponds to the Z-error of the L_α norm between the DEM and the objects. In practice, $\alpha = \frac{3}{2}$ is a good compromise between robustness and sensitivity to the DEM errors.

3.22 A priori The prior density introduces interactions between neighboring objects.It allows to both assemble objects in order to propose a realistic building, and compensate for the lack of information contained in the DEM. A neighborhood relationship on $\mathcal{C}$ must be set up to define the interactions: two distinct quadrilaterals i and $j \in \mathcal{C}$ are said neighbors if they have one common edge. The neighborhood relationship is noticed $\bowtie$ ($i \bowtie j$ represents the set of neighbor pairs of $\mathcal{C}$). In (Lafarge, Descombes, Zerubia, and Pierrot-Deseilligny, 2006b), too many interactions have been set up. Their number must be minimal in order to keep robustness and avoid problems of parameter settings. We propose a simple and efficient prior which is defined through a unique interaction.

To do so, we define an assembling law which tests whether two objects can be assembled together. Two objects $x_i = (m_i, \theta_i)$ and $x_j = (m_j, \theta_j)$ are said "**joinable**" (noticed $x_i \sim_a x_j$) if they verify the three following points:

1 - $\mathcal{F}_i = \mathcal{F}_j$

2 - rooftop orientations are compatible

3 - the common edge of the quadrilateral footprints i and j is not a roof height discontinuity.

The first point verifies that the two models have the same roof form. The second and third points test whether the rooftops of the two objects can be connected.
The prior consists in favoring the "joinable" objects. More precisely, in order to avoid the artefacts, the common parameters of two "joinable" objects are attracted to have similar values. To do so, the unnormalized density h_p is expressed through a Gibbs energy U_p (i.e. $h_p(x) = \exp -U_p(x)$) defined as follows:

$$\forall x \in \mathcal{T},\ U_p(x) = \beta \sum_{i \bowtie j} \mathbb{1}_{\{x_i \sim_a x_j\}} g(x_i, x_j) \quad (5)$$

where $\beta \in \mathbb{R}^+$ is the parameter which weights the importance of the prior density with respect to the likelihood. The function g, living in $[-1, 0]$, measures the distance between the common parameters of two "joinable" objects:

$$g(x_i, x_j) = \frac{D(x_i, x_j)}{D_{max}} - 1 = \frac{\sum_k \omega_k |\widetilde{\theta}_{i,(k)} - \widetilde{\theta}_{j,(k)}|}{D_{max}} - 1 \quad (6)$$

$\widetilde{\theta}_{i,(k)}$ and $\widetilde{\theta}_{j,(k)}$ correspond to the k^{th} element of the set of the common parameters of the objects x_i and x_j respectively. $D_{max} = \max_{x_i, x_j} D(x_i, x_j)$ represents the maximum value of the distance. ω_k are weights which are introduced in this distance in order to normalize the parameter values according to the metric system. These weights are computed knowing the XY and Z resolutions and the configuration of quadrilaterals $\mathcal{C}$.

Fig.4 shows the principle of this interaction. If the two models belong to different roof types (for example a mansard roof model and a semi-elliptic roof model on the top right) or if the two objects do not have compatible roof orientations (see bottom right), they will not be "joinable" and so, the energy will be null. On the contrary, if the two objects are "joinable", the energy will be negative : these configurations are favored. The nearer the parameters of the two objects, the lower the energy. The left configuration is the best one.

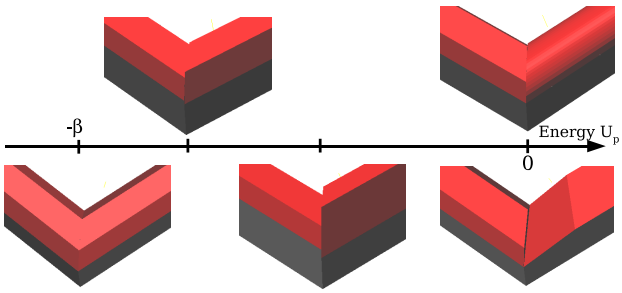

Figure 4. Principle of the prior energy - examples of various interaction cases.

3.3 Optimization

We aim at finding the configuration of objects which maximizes the posterior density $h(.)$, i.e. the Maximum A Posteriori (MAP) estimator x_{MAP}. This is a non convex optimization problem in a high and variable dimension space $\mathcal{T}$ since the models of library $\mathcal{M}$ are defined by a different number of parameters.

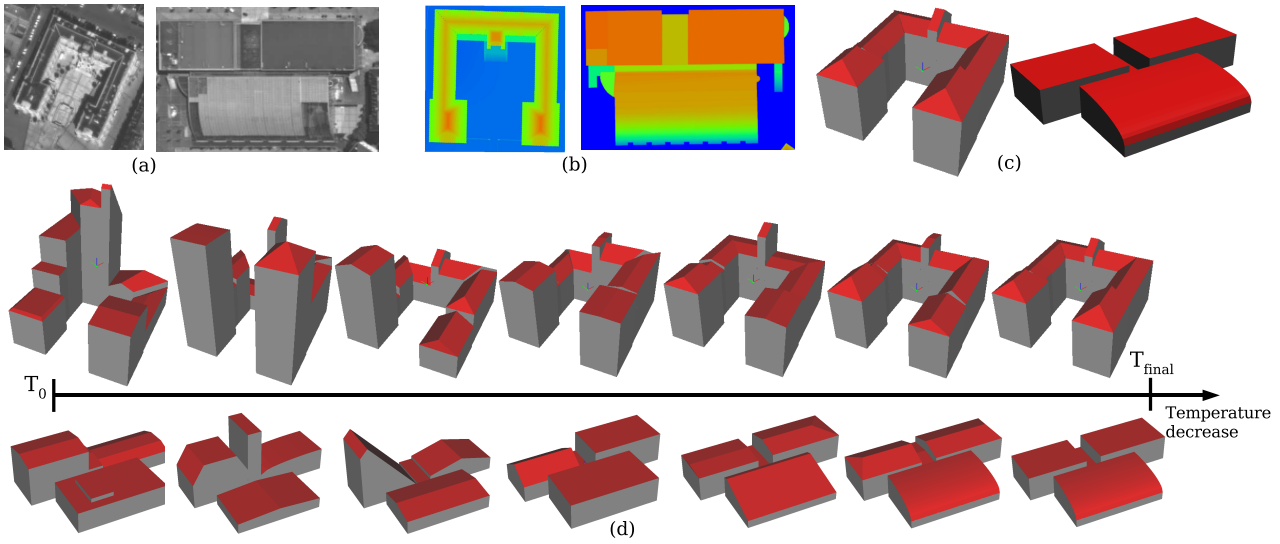

Figure 5. Two simple examples of the optimization process - evolution of the configuration during the temperature decrease **(d)** associated with the satellite images **(a)**, the ground truths **(b)** and the final results **(c)**.

3.31 RJMCMC sampler The Reversible Jump Markov Chain Monte Carlo (RJMCMC) algorithm (Green, 1995) is well adapted to our problem. Several papers have shown the efficiency of the RJMCMC sampler for the problems of multiple parametric object recognition. For example, (Dick, Torr, and Cipolla, 2004) uses such a sampler to reconstruct architectural buildings from terrestrial images where the parametric object set includes structures such as columns, buttresses, entablatures or drainpipes. In (Brenner and Ripperda, 2006), facades are extracted through a grammar based approach driven by a RJMCMC sampler.
The RJMCMC sampler consists in simulating a discrete Markov Chain $(X_t)_{t\in\mathbb{N}}$ on $\mathcal{T}$ having π as invariant measure (specified by the posterior density $h(.)$) which performs small jumps between spaces of variable dimensions respecting the reversibility assumption of the chain.
The jumps are proposed according to three various kernels specified in the following and detailed in (Lafarge, 2007):

- **Kernel Q_1: uniform jumps** It is the most classic kernel consisting in proposing a new state according to uniform distributions. Such a dynamics guaranties that the Markov chain can visit any configuration of the state space. However, using only this kernel, such as in (Lafarge, Descombes, Zerubia, and Pierrot-Deseilligny, 2006b), engenders an important computing time.

- **Kernel Q_2: data-driven jumps** That kernel allows to cleverly explore the state space using a data-driven process, such as in (Tu and Zhu, 2002). To do so, the state x is proposed knowing the data, i.e. according to a probability $p(x|\mathcal{D})$. More precisely, it consists in, firstly, estimating the gutter roof height $\widehat{H_g}$ and the rooftop height $\widehat{H_t}$ of the object concerned by the jump and, secondly, choosing its height parameter values according to the Gaussian distributions $\mathcal{N}(\widehat{H_g},\sigma)$ and $\mathcal{N}(\widehat{H_t},\sigma)$ respectively (in practice, $\sigma = 1$ meter).

- **Kernel Q_3: regularization jumps** In our application, the aesthetic aspect of the result is very important: we need a kernel which proposes well-regularized objects, i.e. objects which are perfectly assembled with their neighbors. The new object x_i must be proposed knowing the neighboring objects $\{x_j/j \bowtie i\}$, i.e. according to $p(x_i|\{x_j/j \bowtie i\})$. The model is uniformly selected according to the models of the neighboring objects. The parameter values are chosen according to Gaussian mixture depending on the parameter values of the neighboring objects.

Let us summarized the RJMCMC sampler. At iteration t, if $X_t = x$:
1- Choose the kernel $Q_i(x,.)$ with probability q_i.
2- According to Q_i, propose a new state y.
3- take $x^{(t+1)} = y$ with probability:

$$\min\left(\frac{\pi(dy)}{\pi(dx)}\frac{Q_i(y,dx)}{Q_i(x,dy)},1\right) \quad (7)$$

and take $x^{(t+1)} = x$ otherwise.

3.32 Simulated annealing A simulated annealing is used to ensure the convergence process: the density $h(.)$ is substituted by $h(.)^{\frac{1}{T_t}}$ where T_t is a sequence of temperatures which tends to zero as t tends to infinity. The simulated annealing allows to theoretically ensure the converge to the global optimum for any initial configuration x_0 using a logarithmic temperature decrease. In practice, we prefer using a geometrical decrease which is faster and gives an approximate solution close to the optimal one. The initial and final temperatures are estimated through the variation of the energy, using the work of (White, 1984).
The decrease process is composed of two stages. At the beginning of the algorithm, i.e. when the temperature is high (see Fig.5-(d) showing two simple examples of simulations), the process explores the density modes and favors the configurations which have a high density. In this exploration stage, the data-driven kernel Q_2 is mainly proposed ($q_2 = 3q_1 = 3q_3 = 0.6$). At low temperature[2], the configuration is close to the optimal solution and does not evolve very much : it consists in a detailed adjustment of the 3D-model parameters. In this second stage, the regularization kernel Q_3 is mainly proposed ($q_3 = 3q_1 = 3q_2$).

[2]In practice, the second stage is detected when the accepted proposition rate computed on 1000 iterations becomes lower than 0.05.

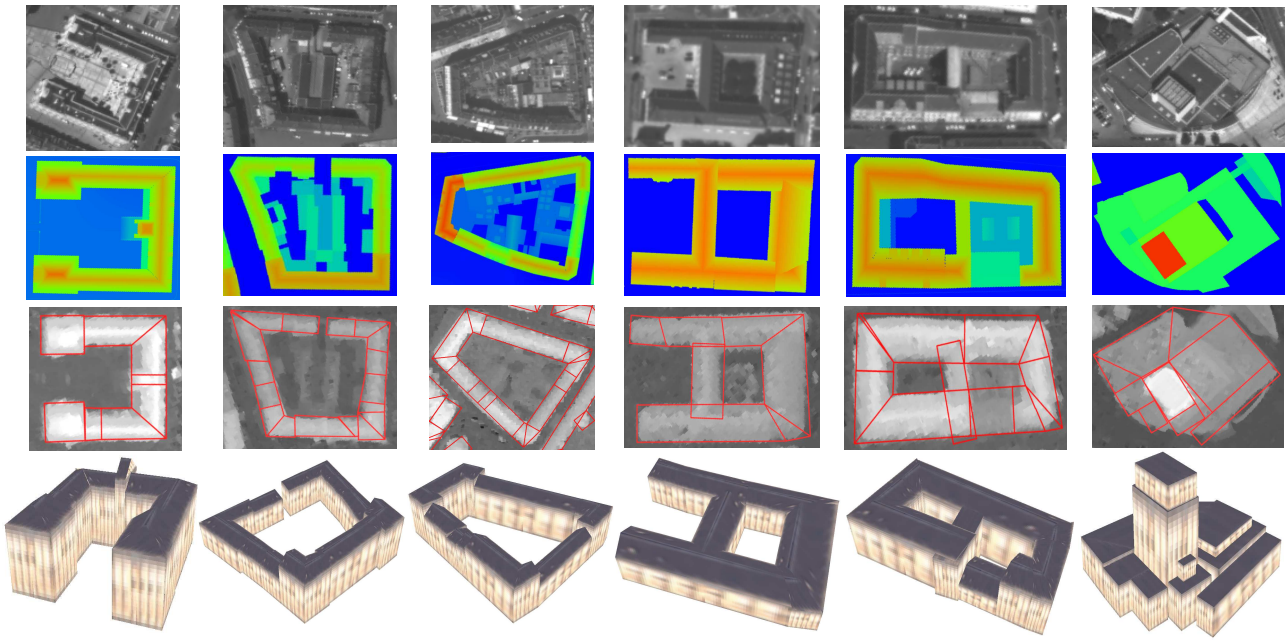

Figure 6. Examples of reconstructed buildings (4^{th} row), satellite images (1^{st} row), ground truths (2^{nd} row) and footprints (3^{rd} row).

4. EXPERIMENTS

The results have been obtained from high resolution satellite images (PLEIADES simulations generated from degraded aerial images by the CNES) on a dense downtown containing an important variety of roof types. DEMs have been generated from 3-view PLEIADES simulations (along track) using a multi-resolution implementation of a Cox and Roy optimal flow matching image algorithm (Roy and Cox, 1998). The ground truths are 3D-models provided by the French Mapping Agency (IGN). Generic textures have been applied on the objects of the scenes for the visualization.

4.1 Results

Fig.6 presents various examples of reconstructed buildings (showing different roof types, roof height discontinuities, closed structures or complex roof junctions) associated with satellite images, ground truths and footprint extraction results. These results are convincing in general. The five first examples provide good descriptions. Even if some details are omitted, the global shapes of buildings are respected compared to ground truths and the generalization level is satisfactory for satellite data in an automatic context. The different roof types are correctly identified. The roof height discontinuities are accurately detected. The 3D-models are correctly assembled as we can see on the 2^{nd} and 3^{rd} examples : it underlines the efficiency of the proposed prior. Few artefacts are generated on the 4^{th} and 5^{th} examples which means the process is adapted to buildings owning complex roof junctions. The last example shows the limits of this approach. Some footprints (especially the curved footprints) cannot be modeled by quadrilateral layouts. Fig.7 shows results on various dense urban areas. These results are aesthetically good compared to results obtained by (Lafarge, Descombes, Zerubia, and Pierrot-Deseilligny, 2006b) on the same scenes.

4.2 Evaluation

The ground errors of these areas provide satisfactory results for satellite data in an automatic context. The over-detection rate (in term of surface) is 9.7%. This rate can be improved by introducing a vegetation mask in the process in order to prevent the detection of trees. The rate of missed detection is quite high (15.3%). However, it is mainly due to low flat buildings of inner courtyards (one floor height structures) that the proposed method cannot detect since these buildings have low DEM discontinuities. Without taking into account these low flat buildings, this rate falls to 4.5%.
Concerning the altimetric evaluation, the global Root Mean Square Error in Z between the reconstructed areas and the 3D ground truth is 2.3 meters (computed on the common building footprints). This value is globally satisfactory compared to the one obtained by (Lafarge, Descombes, Zerubia, and Pierrot-Deseilligny, 2006b) on the same scenes (i.e. 3.2 meters), but remains high. It is mainly due to important local errors which can be explained by several reasons : a non optimal positioning of facades at some locations, inaccuracies in the DEM due to matching problems of non Lambertian surfaces (glass-roof matching,...), and the presence of superstructures (chimneys, dormer windows,...) which are not reconstructed.
The proposed kernels allow to achieve acceptable computing times. For example, less than one minute is necessary to obtain a building of Fig.6 using a 3Ghz processor (*vs* 5 minutes with (Lafarge, Descombes, Zerubia, and Pierrot-Deseilligny, 2006b)).

5. CONCLUSION

The results obtained by the proposed method are convincing : the global shape of buildings is respected and the generalization level is acceptable for satellite data in an automatic context. This approach presents several interesting characteristics such as the automaticity and the robustness. Moreover, it is an adaptive and evolutive method since 3D-models can be added and removed in the library depending on the context.
In future works, it would be interesting to improve the optimization step in order to achieve both precision on the results and lower computing time. Solutions could be to use adaptive cooling schedules in the RJMCMC sampler or to couple this sampler with other dynamics such as the Jump-Diffusion processes. Moreover,

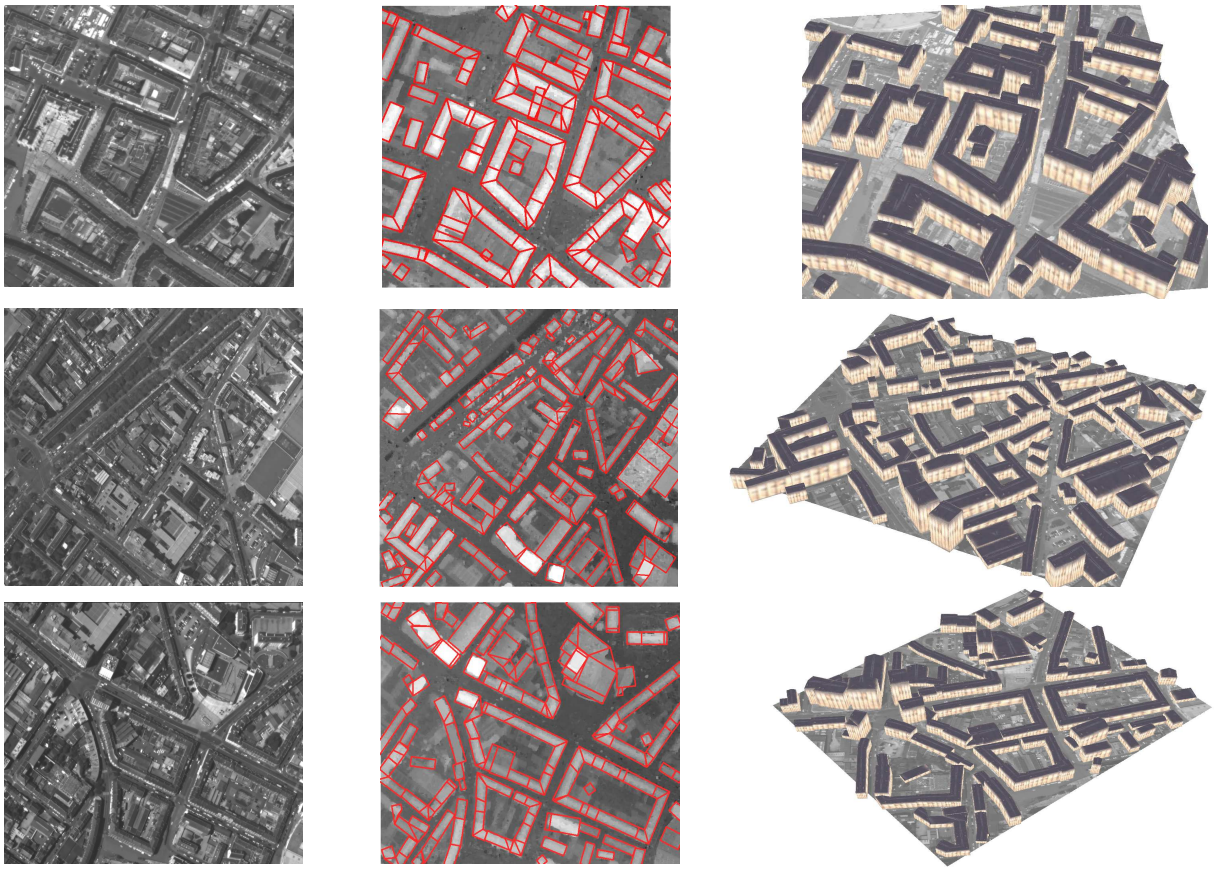

Figure 7. 3D-results on urban areas (3^{rd} row), satellite images (1^{st} row) and quadrilateral footprints (2^{nd} row).

we should evaluate the potential of this method on other kinds of cities such as typical North American urban areas.

REFERENCES

Baillard, C., Schmid, C., Zisserman, A., and Fitzgibbon, A., 1999, Sep). Automatic line matching and 3D reconstruction of buildings from multiple views. In *ISPRS Conference on Automatic Extraction of GIS Objects from Digital Imagery*.

Brenner, C. and Ripperda, N., 2006. Extraction of facades using RJMCMC and constraint equations. In *Proc. of the ISPRS Commission III Symposium on Photogrammetric and Computer Vision*, Bonn, Allemagne.

Dick, A., Torr, P., and Cipolla, R., 2004. Modelling and interpretation of architecture from several images. *International Journal of Computer Vision* 60(2), 111–134.

Green, P., 1995. Reversible Jump Markov Chains Monte Carlo computation and Bayesian model determination. *Biometrika* 57, 97–109.

Haala, N. and Brenner, C., 1999. Extraction of buildings and trees in urban environments. *ISPRS Journal of Photogrammetry and Remote Sensing* 54(2-3), 130–137.

Kim, Z. and Nevatia, R., 2004. Automatic description of complex buildings from multiple images. *Comput. Vis. Image Underst.* 96(1), 60–95.

Lafarge, F., 2007. *Stochastic approaches for 3D building reconstruction*. Ph. D. thesis, Ecole des Mines de Paris, Paris, France.

Lafarge, F., Descombes, X., Zerubia, J., and Pierrot-Deseilligny, M., 2006a. Automatic 3D building reconstruction from DEMs: an application to PLEIADES simulations. In *IAPRS*, Volume XXXVI Part A, pp. 129–136.

Lafarge, F., Descombes, X., Zerubia, J., and Pierrot-Deseilligny, M., 2006b. An automatic building reconstruction method : A structural approach using high resolution images. In *Proc. IEEE ICIP*, Atlanta, USA.

Maas, H. and Vosselman, G., 1999. Two algorithms for extracting building models from raw laser altimetry data. *ISPRS Journal of Photogrammetry and Remote Sensing* 54(2-3), 153–163.

Ortner, M., Descombes, X., and Zerubia, J., 2007, April). Building outline extraction from Digital Elevation Models using marked point processes. *International Journal of Computer Vision* 72(2), 107–132.

Roy, S. and Cox, I., 1998. A maximum-flow formulation of the n-camera stereo correspondence problem. In *Proc. IEEE ICCV*, Bombay.

Scholze, S., Moons, T., and Van Gool, L., 2002. A probabilistic approach to building roof reconstruction using semantic labelling. In *Proceedings of the 24th DAGM Symposium on Pattern Recognition*, London, UK, pp. 257–264.

Taillandier, F. and Deriche, R., 2004. Automatic Builings Reconstruction from Aerial Images : a Generic Bayesian Framework. In *Proc. ISPRS Congress*, Istanbul, Turkey.

Tu, Z. and Zhu, S., 2002. Image Segmentation by Data-Driven Markov Chain Monte Carlo. *IEEE Trans. Pattern Anal. Mach. Intell.* 24(5), 657–673.

Weidner, U. and Forstner, W., 1995. Fowards Automatic Building Reconstruction from High Resolution Digital Elevation Models. *Journal of Photogrammetry and Remote Sensing* 50(4), 38–49.

White, S., 1984. Concepts of scale in simulated annealing. In *Proc. IEEE Int. Conf. on Computer Design*.